Sensorless Control of SynRM Based on Dual-oriented Active EMF models and Adaptive Fading Kalman Filter

Fengtao Gao[1], Zhonggang Yin[1], Cong Bai[1], and Yanqing Zhang[1]
[1] Xi'an University of Technology, China

***Abstract*-- The tracking performance of a position sensorless synchronous reluctance motor (SynRM) drive suffers from the inductance mismatch significantly. In case of mismatched inductance occur in the drive, the estimated position deviates from the actual value significantly in the conventional active EMF (AEMF) model-based position observer as the load increases. A sensorless control strategy based on the dual-oriented AEMF (DO-AEMF) and adaptive fading Kalman filter (AFKF) is proposed to suppress the problem. The AEMF models of SynRM are developed at the *d*-axis and *q*-axis, which have different parameter sensitivity. Then, the AFKF observers are built based on the two models. The advantages of the two observers are combined to abate the bad effect on position estimation to the greatest extent. Moreover, the different AEMF models work under different load conditions and switch according to current vector angle. Last, the proposed strategy is implemented on a 1.5 kW SynRM experiment prototype.**

***Index Terms*-- Synchronous reluctance motor, sensorless control, adaptive fading Kalman filter, AEMF models.**

I. INTRODUCTION

Synchronous reluctance motor (SynRM) has been vigorously promoted in industrial applications, such as compressors, machine spindles, etc. This largely depends on SynRM's low cost, low loss, and high reliability [1]. SynRM drive without a position sensor has always been the focus of academic and industrial research over recent years since it helps to benefit industrial users in prime cost and production. The two most concerned methods in academia are the high-frequency signal injection [2] and the fundamental frequency model [3,4]. In industrial applications, the EMF-based methods, including flux observer, extended EMF (EEMF), and active EMF, are commonly used in a sensorless SynRM drive, thanks to the characteristics of simplicity, and no audible noise. Flux observer has simple mathematical expression and minimal parameter dependency. Nevertheless, it needs to integrate the back EMF, which brings about the DC component in the estimated flux. The low-pass filter (LPF) and second-order generalized integrator (SOGI) are the alternative solutions to alleviate the problem [5].

EEMF is the typical sensorless control scheme for a SynRM. In [6], a sensorless control method of SynRM based on EEMF is developed by S. Ichikawa *et al.* Different from the traditional definition of *d*-axis (direction of maximum inductance L_d), the direction of L_q is stipulated as the *d*-axis. The minimal-order stator observer is employed to track the true EEMF. Zhao *et al* derive the extended flux model from the voltage equations of SPMSM by defining the flux concept [7]. The model is also called AEMF model, which processes the less parameters and simpler structure than EEMF model. In [8,9], the AEMF method is popularized to sensorless SynRM drive.

To get a high-performance AEMF estimation, several kinds of observers are studied in recent years, which cover state observer [10], model reference adaptive system (MRAS) [11], sliding mode observer (SMO) [12], and Kalman filter. The state observer has the superiorities of the simple model and mature parameter determination method to ensure system stability, but the observation suffers from parameter change and measurement noise. Designing the MRAS is based on the stability theory, in which the adaptive laws are selected from the perspective of ensuring system stability, so it is easy to ensure system stability. SMO is known for its easy-implemented pattern and excellent robustness, as the nonlinear sliding mode function is introduced into the observer. In application, suppression of the chatting and phase delay brought by the low-pass filter are key issues.

Kalman filter (KF) is developed on the basis of the statistical characteristics of variables in a discrete system and has natural noise resistance and high estimation accuracy. In the field of AC motor control, KF is often exploited to directly estimate the speed and position of the induction motor or SPMSM [13,14]. For interior PMSM and SynRM, the mathematical model cannot contain both rotor position and speed variables. Therefore, the speed and position are hard to be estimated by extending them in the state equation. In [15], a nonlinear model of SynRM is developed and the extended Kalman filter (EKF) is exploited to estimate the state. The authors develope a state space model based on speed and position in $\alpha\beta$ frame, just like the SPMSM modeling method. Although the model that only contains the speed can be developed and the rotor position easy to gain through integrating the speed, the calculated position is sensitive to the noise and the biased L_d and L_q. Therefore, the rotor position and speed information can only be obtained by estimating the EEMF or AEMF when the KF observer is employed. In practice, the fixed noise covariance matrix of KF makes the method optimal under a single operating condition. When the operating condition changes, the same estimation accuracy cannot be guaranteed. Moreover, the position estimation

This work is supported in part by the National Natural Science Foundation of China under Grant 52207222 and 52207016, in part by Shaanxi Outstanding Youth Fund under Grant 2020JC-40, in part by Nature Science Basic Research Plan in Shaanxi Province under Grant 2021JQ-477, 2022JQ-538 and 2022GY-016, in part by Key Research and Development Project of Shaan Xi Province under Grant 2021GY-282, in part by China Postdoctoral Science Foundation under Grant 2021M702640, and in part by the Nature Science Basic Research Plan in Shaanxi Province under Grant 2021JQ477.

error increases as the current vector angle increase under the inductance mismatch [16].

In this paper, a sensorless control method for SynRM based on an adaptive fading Kalman filter and dual-oriented AEMF models is proposed. First, the Kalman filter gain is adjusted adaptively by introducing the fading factor into the error covariance matrix. Then, the parameter sensitivity of the AFKF-based AEMF observer is analyzed, and the $L_{\min}$-oriented AEMF model is derived by selecting the direction of the minimum inductance value as the d-axis. We found that the position estimation error curve of the AEMF models constructed by selecting different coordinate systems is different. Last, the $L_{\max}$-oriented AEMF model and the $L_{\min}$-oriented AEMF model are employed to establish the AFKF observer, and the evaluation function based on the current angle is designed for switching the AFKF observers. The effectiveness of the proposed strategy is validated with a 1.5 kW SynRM drive system.

II. Sensorless Control Based on Dual-Oriented AEMF Models and AFKF

A. Mathematical model of SynRM

The ideal mathematical model of a SynRM in dq frame is given by

$$\begin{bmatrix} u_d \\ u_q \end{bmatrix} = \begin{bmatrix} R_s + L_d p & -\omega_{re} L_q \\ \omega_{re} L_d & R_s + L_q p \end{bmatrix} \begin{bmatrix} i_d \\ i_q \end{bmatrix} \tag{1}$$

where u_d, u_q, i_d, and i_q are the stator voltages and stator currents. R_s is the stator resistance, ω_{re} is the electromagnetic angular speed, the p denotes differential operator. The above equation is found on the base of

$$\begin{bmatrix} \psi_d \\ \psi_q \end{bmatrix} = \begin{bmatrix} L_d & 0 \\ 0 & L_q \end{bmatrix} \begin{bmatrix} i_d \\ i_q \end{bmatrix} \tag{2}$$

where ψ_d and ψ_q are the stator flux, L_d and L_q are the apparent stator inductances.

The electromagnetic torque equation of a SynRM can be derived as

$$T_e = 1.5 n_p (L_d - L_q) i_d i_q \tag{3}$$

where n_p is the number of pole pairs.

The mechanical equations of the SynRM drive system are given by

$$J \frac{d\omega_{rm}}{dt} = T_e - T_L - B_m \omega_{rm} \tag{4}$$

$$p\theta_{re} = \omega_{re} \tag{5}$$

where $\omega_{rm} = \omega_{re}/n_p$ is the mechanical angular speed, θ_{re} is the rotor position.

B. Dual-oriented AEMF models

The dual-oriented coordinate system is displayed as Fig. 1, where the blue arrow denotes the direction of the extreme value of the inductance around the rotor, and the red arrow denotes dq coordinate system. To distinguish the two coordinate systems, the conventional coordinate system is marked as dq, while the new coordinate system is marked as $d'q'$.

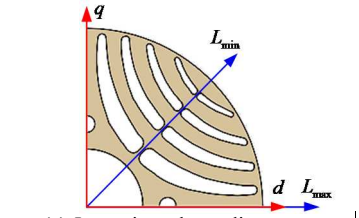

(a) $L_{\max}$-oriented coordinate system

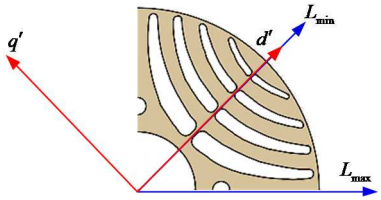

(b) $L_{\min}$-oriented coordinate system

Fig. 1. Definition of the dual-oriented coordinate system

By using the reverse Park coordinate transformation, based on (1), the conventional AEMF model of a SynRM under the $L_{\max}$-oriented coordinate system is given by

$$\begin{bmatrix} u_\alpha \\ u_\beta \end{bmatrix} = \begin{bmatrix} R_s + pL_q & 0 \\ 0 & R_s + pL_q \end{bmatrix} \begin{bmatrix} i_\alpha \\ i_\beta \end{bmatrix} + \begin{bmatrix} e_\alpha^{\max} \\ e_\beta^{\max} \end{bmatrix} \tag{6}$$

$$\begin{bmatrix} e_\alpha^{\max} \\ e_\beta^{\max} \end{bmatrix} = \omega_{re} \psi_{ext}^{\max} \begin{bmatrix} -\sin\theta_{re} \\ \cos\theta_{re} \end{bmatrix} \tag{7}$$

where, $\psi_{ext}^{\max} = (L_d - L_q) i_d$, The above model is called the steady-state $L_{\max}$-oriented AEMF model. u_α, u_β, i_α, and i_β are the stator voltages and stator currents under $\alpha\beta$ frame, in which α-axis coincides with the direction of $L_{\max}$.

The voltage equation (1) can be rewritten as (8) when the $L_{\min}$-oriented coordinate system is employed.

$$\begin{bmatrix} u_d' \\ u_q' \end{bmatrix} = \begin{bmatrix} R_s + L_q p & -\omega_{re} L_d \\ \omega_{re} L_q & R_s + L_d p \end{bmatrix} \begin{bmatrix} i_d' \\ i_q' \end{bmatrix}. \tag{8}$$

where u_d', u_q', i_d', i_q' are the stator voltages and stator currents under $d'q'$ frame.

In this case, the steady-state $L_{\min}$-oriented AEMF model can be derived as

$$\begin{bmatrix} u_\alpha' \\ u_\beta' \end{bmatrix} = \begin{bmatrix} R_s + pL_d & 0 \\ 0 & R_s + pL_d \end{bmatrix} \begin{bmatrix} i_\alpha' \\ i_\beta' \end{bmatrix} + \begin{bmatrix} e_\alpha^{\min} \\ e_\beta^{\min} \end{bmatrix} \tag{9}$$

$$\begin{bmatrix} e_\alpha^{\min} \\ e_\beta^{\min} \end{bmatrix} = \omega_{re} \psi_{ext}^{\min} \begin{bmatrix} \cos\theta_{re} \\ -\sin\theta_{re} \end{bmatrix} \tag{10}$$

where, $\psi_{ext}^{\min} = (L_d - L_q) i_d'$. u_α', u_β', i_α', and i_β' are the stator voltages and stator currents under $\alpha'\beta'$ frame, in which α'-axis coincides with the direction of $L_{\min}$. The phases of the two AEMFs differ by 90 deg, and they have different amplitudes. It is important to estimate the two AEMFs with high performance.

The Kalman filter is capable to estimate the states under noisy working conditions. However, it is troublesome to adjust the parameters of the noise covariance matrix. Next, the adaptive fading Kalman filter is designed to estimate the two AEMFs.

C. Design of AFKF observers

The AFKF takes the advantage of less sensitivity to the noise covariance matrix ($\boldsymbol{P}_0$, $\boldsymbol{Q}$, and $\boldsymbol{R}$) and strong adaptability to the working condition change. In this paper, two AFKFs are employed to estimate the AEMFs in the $L_{\max}$-oriented AEMF model and the $L_{\min}$-oriented AEMF model. We select the state variables as

$$\boldsymbol{x}=(i_\alpha,i_\beta,e_\alpha^{\max},e_\beta^{\max})^{\mathrm{T}},\ \boldsymbol{x}'=(i'_\alpha,i'_\beta,e_\alpha^{\min},e_\beta^{\min})^{\mathrm{T}} \tag{11}$$

The state space equations of the two models are given by

$$\begin{cases} p\boldsymbol{x}=\boldsymbol{A}\boldsymbol{x}+\boldsymbol{B}\boldsymbol{u} \\ \boldsymbol{y}=\boldsymbol{C}\boldsymbol{x} \end{cases} \tag{12}$$

$$\begin{cases} p\boldsymbol{x}'=\boldsymbol{A}'\boldsymbol{x}'+\boldsymbol{B}'\boldsymbol{u} \\ \boldsymbol{y}'=\boldsymbol{C}'\boldsymbol{x}' \end{cases} \tag{13}$$

where, $\boldsymbol{u}=(u_\alpha,u_\beta)^{\mathrm{T}}$ is input vector, $\boldsymbol{y}=(i_\alpha,i_\beta)^{\mathrm{T}}$ and $\boldsymbol{y}'=(i'_\alpha,i'_\beta)^{\mathrm{T}}$ are the output vector, and

$$\boldsymbol{A}=\begin{bmatrix} -\frac{R_s}{L_q} & 0 & -\frac{1}{L_q} & 0 \\ 0 & -\frac{R_s}{L_q} & 0 & -\frac{1}{L_q} \\ 0 & 0 & 1 & -\omega_{re} \\ 0 & 0 & \omega_{re} & 1 \end{bmatrix},\boldsymbol{B}=\begin{bmatrix} \frac{1}{L_q} & 0 \\ 0 & \frac{1}{L_q} \\ 0 & 0 \\ 0 & 0 \end{bmatrix},$$

$$\boldsymbol{A}'=\begin{bmatrix} -\frac{R_s}{L_d} & 0 & -\frac{1}{L_d} & 0 \\ 0 & -\frac{R_s}{L_d} & 0 & -\frac{1}{L_d} \\ 0 & 0 & 1 & -\omega_{re} \\ 0 & 0 & \omega_{re} & 1 \end{bmatrix},\boldsymbol{B}'=\begin{bmatrix} \frac{1}{L_d} & 0 \\ 0 & \frac{1}{L_d} \\ 0 & 0 \\ 0 & 0 \end{bmatrix},$$

$$\boldsymbol{C}=\boldsymbol{C}'=\begin{bmatrix} 1 & 0 & 0 & 0 \\ 0 & 1 & 0 & 0 \end{bmatrix}^{\mathrm{T}}.$$

The AFKF observers can be designed as

1) One-step state prediction

$$\tilde{\boldsymbol{x}}_k^i=\boldsymbol{A}_k^i\hat{\boldsymbol{x}}_{k-1}^i+\boldsymbol{B}_k^i\boldsymbol{u}_k \tag{14}$$

$$\tilde{\boldsymbol{P}}_k^i=\lambda_k^i\boldsymbol{A}_k^i\hat{\boldsymbol{P}}_{k-1}^i(\boldsymbol{A}_k^i)^{\mathrm{T}}+\boldsymbol{Q}_k^i \tag{15}$$

where $i=1,2$ denotes the $L_{\max}$-oriented AEMF model and $L_{\min}$-oriented AEMF model, respectively.

2) *State correction based on the innovation*

$$\hat{\boldsymbol{x}}_k^i=\tilde{\boldsymbol{x}}_k^i+\boldsymbol{K}_k^i(\boldsymbol{y}_k^i-\boldsymbol{H}\tilde{\boldsymbol{x}}_k^i) \tag{16}$$

$$\hat{\boldsymbol{P}}_k^i=(\boldsymbol{I}-\boldsymbol{K}_k^i\boldsymbol{H})\tilde{\boldsymbol{P}}_k^i \tag{17}$$

$$\boldsymbol{K}_k^i=\tilde{\boldsymbol{P}}_k^i\boldsymbol{H}^T\left(\boldsymbol{H}_k\tilde{\boldsymbol{P}}_k^i\boldsymbol{H}^T+\boldsymbol{R}_k^i\right)^{-1} \tag{18}$$

3) *Update the adaptive fading factors*

$$\lambda_k^i=\max\{1,\mathrm{tr}(\boldsymbol{N}_k^i)/\mathrm{tr}(\boldsymbol{M}_k^i)\} \tag{19}$$

$$\boldsymbol{M}_k^i=\boldsymbol{H}\boldsymbol{A}_{k-1}^i\hat{\boldsymbol{P}}_{k-1}^i(\boldsymbol{A}_{k-1}^i)^{\mathrm{T}}\boldsymbol{H}^T \tag{20}$$

$$\boldsymbol{N}_k^i=\bar{\boldsymbol{C}}_k^i-\boldsymbol{R}_k^i-\boldsymbol{H}\boldsymbol{Q}_k^i\boldsymbol{H}^T \tag{21}$$

$$\bar{\boldsymbol{C}}_k^i=\begin{cases} 0.5\boldsymbol{\varepsilon}_0^i(\boldsymbol{\varepsilon}_0^i)^{\mathrm{T}}, & k=0 \\ \dfrac{\lambda_k\boldsymbol{\varepsilon}_0^i(\boldsymbol{\varepsilon}_0^i)^{\mathrm{T}}}{1+\lambda_k^i}, & k=1,2,3\ldots \end{cases} \tag{22}$$

$$\boldsymbol{\varepsilon}_k^i=\boldsymbol{y}_k-\boldsymbol{H}\tilde{\boldsymbol{x}}_k^i. \tag{23}$$

where λ_k^i are the adaptive fading factors, $\boldsymbol{\varepsilon}_k^i$ are the innovations, and the $\bar{\boldsymbol{C}}_k^i$ are the estimated innovation covariances.

D. Parameter sensitivity analysis

We define the mismatched inductance as $\bar{L}_d=L_d+\Delta L_d$, $\bar{L}_q=L_q+\Delta L_q$, where ΔL_d and ΔL_q are the inductance deviations. Taking the AFKF based on $L_{\max}$-oriented AEMF model as an example, the Kalman filter gain matrices can be written as

$$\boldsymbol{K}=\begin{bmatrix} \beta_1 & 0 & \beta_2 & 0 \\ 0 & \beta_1 & 0 & \beta_2 \end{bmatrix}^{\mathrm{T}}. \tag{24}$$

In complex frequency domain, the observer with mismatched parameters is modeled as

$$\begin{cases} s\hat{\boldsymbol{i}}_{\alpha\beta}=\dfrac{1}{\bar{L}_q}\left(\boldsymbol{u}_{\alpha\beta}-\bar{R}_s\hat{\boldsymbol{i}}_{\alpha\beta}-\hat{\boldsymbol{e}}_{\alpha\beta}\right)+\beta_1\left(\boldsymbol{i}_{\alpha\beta}-\hat{\boldsymbol{i}}_{\alpha\beta}\right) \\ s\hat{\boldsymbol{e}}_{\alpha\beta}=j\hat{\omega}_{re}\hat{\boldsymbol{e}}_{\alpha\beta}+\beta_2\left(\boldsymbol{i}_{\alpha\beta}-\hat{\boldsymbol{i}}_{\alpha\beta}\right) \end{cases} \tag{25}$$

When the SynRM drive system operates in steady state, $\hat{\omega}_{re}=\omega_{re}$ holds, and the current estimation error vector at steady state is

$$s\hat{\boldsymbol{e}}_{\alpha\beta}=j\hat{\omega}_{re}\hat{\boldsymbol{e}}_{\alpha\beta}+\beta_2\left(\boldsymbol{i}_{\alpha\beta}-\hat{\boldsymbol{i}}_{\alpha\beta}\right)\Rightarrow\boldsymbol{i}_{\alpha\beta}-\hat{\boldsymbol{i}}_{\alpha\beta}=0 \tag{26}$$

Then, the AEMF estimation error vector can be derived as

$$\boldsymbol{e}_{\alpha\beta}-\hat{\boldsymbol{e}}_{\alpha\beta}=(\Delta R_s+\Delta L_q s)\boldsymbol{i}_{\alpha\beta} \tag{27}$$

It can be seen from (27) that when the motor parameters are accuracy, the AFKF observer can be used to estimate AEMF without static error. In error analysis, it is not enough to get the estimation error of the AEMF. Since the estimated rotor position is extracted from the estimated AEMF through the PLL, it is particularly important to analyze the phase error of the estimated AEMF. The quantitative analysis will be carried out by means of phasor diagrams.

For the convenience of analysis, the impact of stator resistance is ignored. Then, the phasor diagrams of position estimation error production under different ranges of the current vector angle are depicted in Fig. 2. It can be observed that a position estimation error emerges when the estimated AEMF has an error compared with the actual AEMF. As is depicted in Fig. 2(a), the position estimation error of the $L_{\max}$-oriented AEMF model can be derived as

$$\begin{aligned} \Delta\theta'_{re}&=\arctan\frac{\omega_{re}\Delta L_q|\boldsymbol{i}|\sin(\theta_i)}{\omega_{re}(L_d-L_q)i_d-\omega_{re}\Delta L_q|\boldsymbol{i}|\cos(\theta_i)} \\ &=\arctan\frac{\Delta L_q\sin(\theta_i)}{(L_d-L_q)\cos(\theta_i)-\Delta L_q\cos(\theta_i)} \end{aligned}. \tag{28}$$

where θ_i is the current angle, defined as $\theta_i=i_q/i_d$. The position estimation error of the AFKF built on the $L_{\min}$-oriented AEMF model can be deduced by the same method as

$$\Delta\theta''_{re} = \arctan\frac{-|\Delta\boldsymbol{e}'|\sin(\theta'_i)}{|\boldsymbol{e}'|+|\Delta\boldsymbol{e}'|\cos(\theta'_i)} = \arctan\frac{-\Delta L_d\sin(\theta'_i)}{(L_d-L_q)\cos(\theta'_i)+\Delta L_d\cos(\theta'_i)} \quad (29)$$

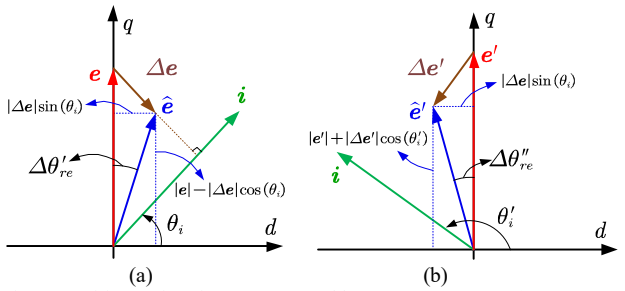

Fig. 2. Position estimation error caused by an error vector. (a) L_{max}-oriented AEMF model (b) L_{min}-oriented AEMF model

Fig. 3 shows the position estimation errors when the inductance parameter mismatches with the actual value. It can be observed that the L_{max}-oriented AEMF model makes a larger position estimation error in the MTPA operating area than that of the L_{min}-oriented AEMF model. The L_{min}-oriented AEMF model could be a better choice for the MTPA operating area. In fact, a minimum excitation current has to be set in the sensorless control system of SynRM, which means the motor has to operate in a non-MTPA area. In this case, the L_{max}-oriented AEMF model could be a better choice. Therefore, the two models are employed to design the AFKF observer.

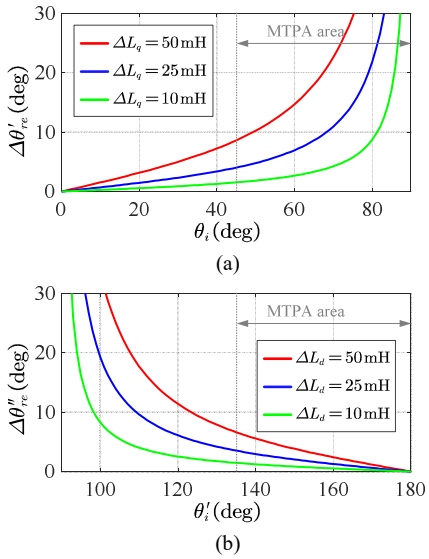

Fig. 3. Position estimation errors under inductance mismatch. (a) L_{max}-oriented AEMF model, (b) L_{min}-oriented AEMF model.

According to the different relationships between position estimation error and current angle, it is reasonable to choose an active AEMF observer by the current angle-based evaluation function. The framework of the position estimation and switching strategy is displayed in Fig. 4. The speeds and the rotor positions are extracted by the normalized quadrature phase-locked loop (NQPLL), which are presented in Fig. 5 and Fig. 6. To avoid frequent switching between two observers at θ_i=45 deg or θ_i=135 deg, the hysteresis control strategy is exploited. Moreover, since the position estimation errors of the two observers are not equal at the switching point, it is necessary to design a weighted fusion method for two estimated positions and speeds.

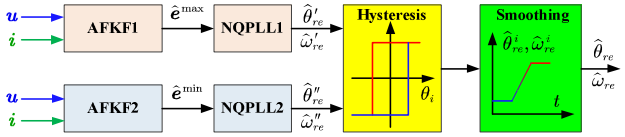

Fig. 4. The framework of the position estimation and switching strategy.

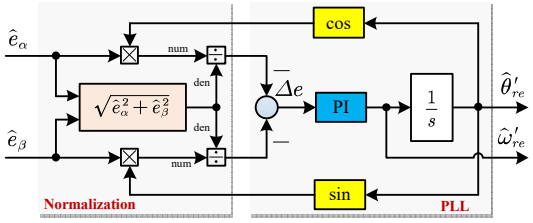

Fig. 5. The framework diagram of the NQPLL1.

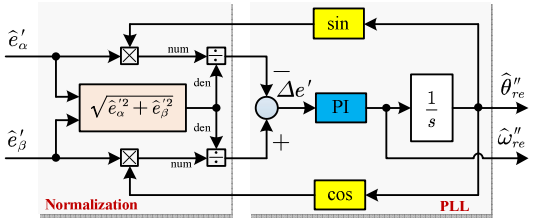

Fig. 6. The framework diagram of the NQPLL2.

The block SynRM sensorless control on the basis of DO-AEMF and AKFK observers is illustrated in Fig. 5. The typical field-oriented control is the basic control framework, consisting of maximum torque per ampere (MTPA) control, coordinate transformations, SVPWM generation, speed controller, current controllers, and position estimation strategy.

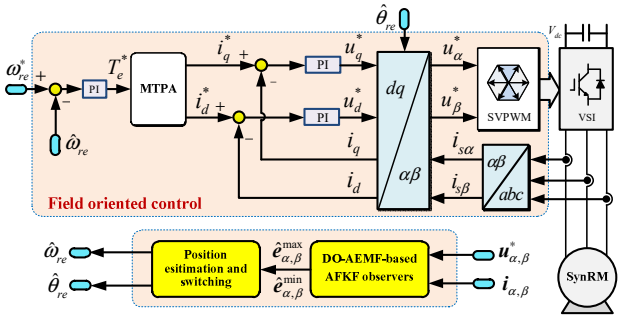

Fig. 7. Sensorless control system of SynRM based on the DO-AEMF and AFKF observers.

III. Experimental Verification

A. Experimental platform

To validate the availability of the proposed method, some experimental tests are carried out at a SynRM drive system based on TI TMS320F28335 DSP. The experiment prototype is displayed in Fig. 8. The SynRM drive system consists of a 1.5 kW SynRM, voltage source inverter (VSI), control circuit, resolver, operation panel, simulator, and upper computer. The servo loading system includes a servo motor, a servo driver, and a braking resistor. The switching frequency of the VSI is 5 kHz, the sampling interval of the proposed method in the experiment is 200 μs, by which the sampling interval of the sensorless control algorithm

follows. The nominal parameters of the tested SynRM are listed in Table I. The off-line identified inductance-current surfaces are shown in Fig. 9. To effectuate the AFKFs based on DO-AEMF, the L_d and L_q surfaces are tabulated in the microprocessor, and the look-up table is achieved to avoid the position estimation error made by the magnetic saturation and cross-saturation effect.

The parameters of the AEMF observers are as follows: $\boldsymbol{P}_0$=diag(0.1, 0.1, 1, 1), $\boldsymbol{Q}$=diag(10^{-4}, 10^{-4}, 0.5, 0.5), $\boldsymbol{R}$=diag(0.05, 0.05). It is noted that the determination of the noise covariance matrices has a wide tolerance since AFKF is concerned with adjusting the Kalman gain by fading factors.

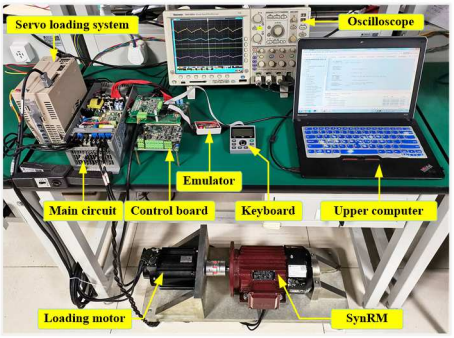

Fig. 8. The experimental platform of 1.5 kW SynRM.

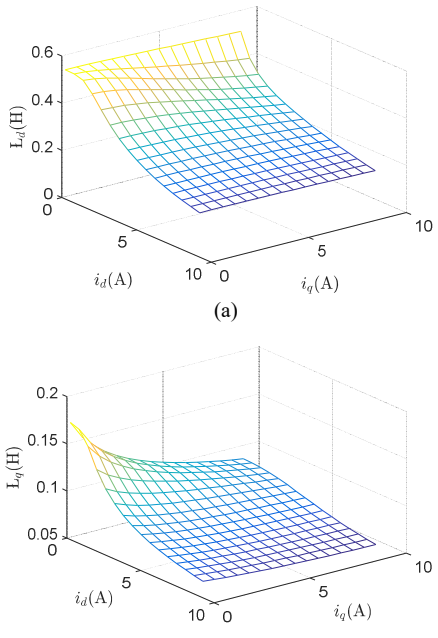

Fig. 9. The inductance versus i_d and i_q of the tested SynRM. (a) L_d map, (b) L_q map.

TABLE I
PARAMETERS OF THE TESTED SYNRM

Parameters	Values
Rated voltage	340 V
Rated current	4.4 A
Rated power	1.5 kW
Rated speed	1500 rpm
Rated torque	9.5 N·m
Rtator resistance	2.8 Ω
Moment of inertia	0.02 kg·m^2
Number of pole pairs	2

B. Experimental results

To validate the correctness of the proposed sensorless method, the behavior of the L_{max}-oriented AEMF model-based AFKF and the L_{min}-oriented AEMF model-based AFKF observer is tested by experiments. Fig. 10 displays the experimental results when the sensorless control system operates at 1500 rpm under no-load operation. The given excitation minimum current is set as 2 A. The estimated AEMFs, actual rotor position, and position estimation error are displayed in each subfigure. For a better presentation, the estimated AEMFs are normalized to 1. We can find that the two observers are able to track the real rotor position well. Moreover, the results prove that the inductance parameters identified offline are accurate.

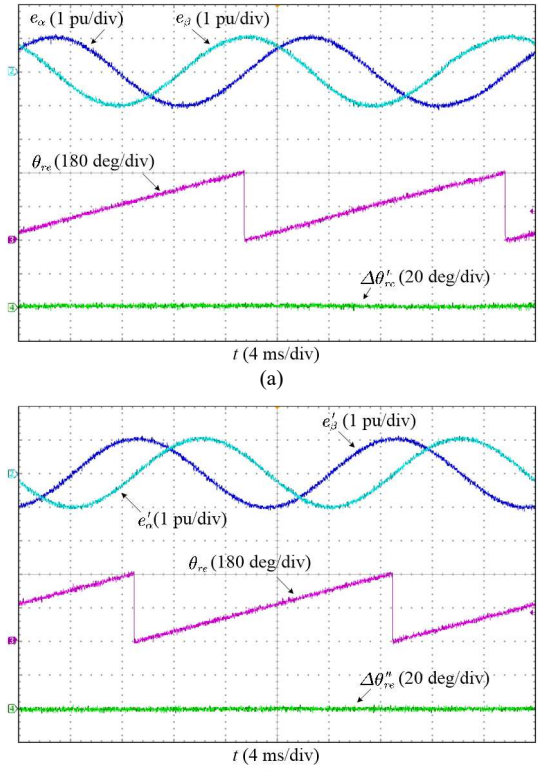

Fig. 10. Experimental results of the sensorless control system at 1500 rpm under no load without inductance mismatch. (a) L_{max}-oriented AEMF model-based AFKF, (b) L_{min}-oriented AEMF model-based AFKF.

For inspecting the switching process between two observers, a loading experiment is carried out. The given minimum excitation current is set as 2 A. Fig. 11 presents the experimental results of the sensorless control system at 1500 rpm with a rated step-load disturbance. In the results, the actual speed, the AEMF model flag (0 denotes L_{max}-oriented AEMF model, 1 denotes L_{min}-oriented AEMF model), final position estimation error, and phase current are displayed, from top to bottom. The result indicates that the switching and smoothing strategy works well during the loading transient. The switch of the model does not cause an abnormality of position estimation error, as the linear smoothing algorithm provides useful estimation results.

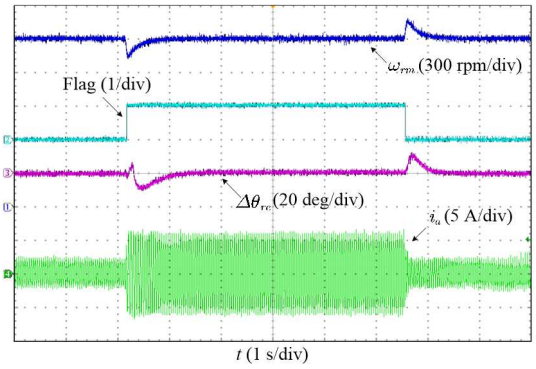

Fig. 11. Experimental results of the sensorless control system at 1500 rpm with a rated step-load disturbance.

To validate the effectiveness of the proposed method under the condition of the inductance of the SynRM mismatches with that of in drive control system, we change the inductances in the control system with an increment of 25 mH. Fig. 12 and Fig. 13 display the experimental results of the sensorless control system under the inductances mismatch, and the no-load and rated-load conditions are implemented, respectively. In Fig. 12, the given minimum excitation current is set as 0.5 A. The L_{max}-oriented AEMF model is active under the no-load condition, while the L_{min}-oriented AEMF model is active under the rated-load condition. The results indicate that the proposed method processes an excellent estimation performance in comparison with that of the single-oriented AEMF model-based sensorless control method.

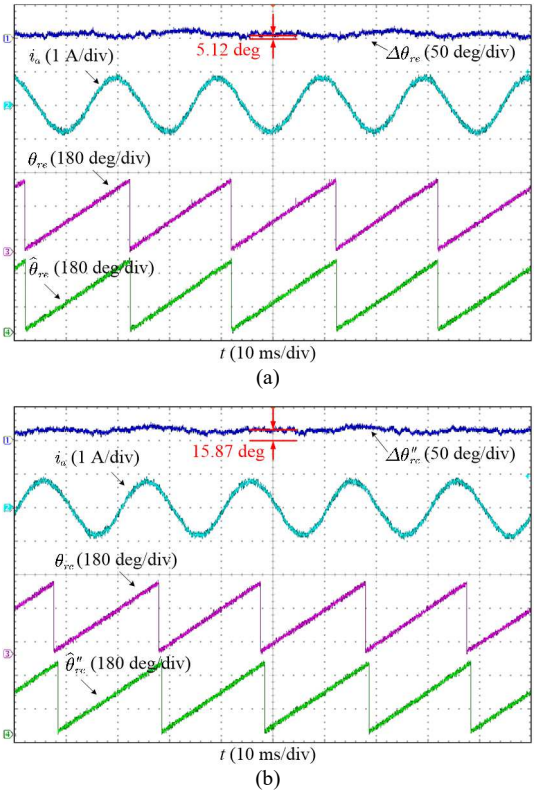

Fig. 12. Experimental results of the sensorless control system under no load with inductance mismatch. (a) AFKF based on DO-AEMF model under ΔL_q=25mH. (b) AFKF based on the L_{min}-oriented AEMF model under ΔL_d=25mH.

As depicted in Fig. 12, we can find that when the SynRM is not loaded, the average position estimation error based on the DO-AEMF model is about 5.12 deg, while the error based on the L_{min}-oriented AEMF model is about 15.87 deg. It can be seen from Fig. 13 that, when the SynRM is loaded with rated torque, the average position estimation error based on the L_{max}-oriented AEMF model is about 22.05 deg, while the error based on the DO-AEMF model is about 5.91 deg.

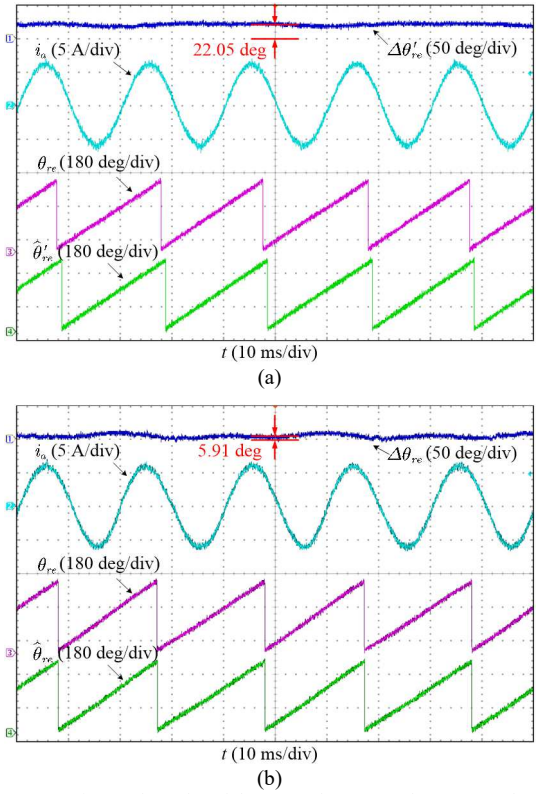

Fig. 13. Experimental results of the sensorless control system under rated load with inductance mismatch. (a) AFKF based on the L_{max}-oriented AEMF model under ΔL_q=25mH. (b) AFKF based on DO-AEMF model under ΔL_d=25mH.

IV. Conclusions

In this paper, the sensorless control method based on the dual-oriented AEMF model and AFKF is proposed. The L_{max}-oriented AEMF model and the L_{min}-oriented AEMF model have different estimation performances under different loading conditions, and the proposed method switches the two models according to the current vector angle adaptively. The behaviour of the proposed method is validated in the experiment. It is proved that the proposed method, who covers the whole current vector angle, has a better capability to inhibit the inductance parameter mismatch, compared to the observer based on single-oriented AEMF model.

References

[1] M. Murataliyev, M. Degano, M. Di Nardo, N. Bianchi and C. Gerada, "Synchronous Reluctance Machines: A Comprehensive Review and Technology Comparison," in *Proceedings of the IEEE*, vol. 110, no. 3, pp. 382-399, March 2022.

[2] C. Li, G. Wang, G. Zhang, N. Zhao and D. Xu, "Adaptive Pseudorandom High-Frequency Square-Wave Voltage Injection Based Sensorless Control for SynRM Drives," in *IEEE Transactions on Power Electronics*, vol. 36, no. 3, pp. 3200-3210, March 2021.

[3] A. Varatharajan, G. Pellegrino, E. Armando and M. Hinkkanen, "Sensorless Synchronous Motor Drives: A Review of Flux Observer-Based Position Estimation Schemes Using the Projection Vector Framework," in *IEEE Transactions on Power Electronics*, vol. 36, no. 7, pp. 8171-8180, July 2021.

[4] D. Pasqualotto, S. Rigon and M. Zigliotto, "Sensorless Speed Control of Synchronous Reluctance Motor Drives based on Extended Kalman Filter and Neural Magnetic Model," in *IEEE Transactions on Industrial Electronics*. doi: 10.1109/TIE.2022.3159962

[5] W. Xu, Y. Jiang, C. Mu and F. Blaabjerg, "Improved Nonlinear Flux Observer-Based Second-Order SOIFO for PMSM Sensorless Control," in *IEEE Transactions on Power Electronics*, vol. 34, no. 1, pp. 565-579, Jan. 2019.

[6] S. Ichikawa, M. Tomita, S. Doki and S. Okuma, "Sensorless Control of Synchronous Reluctance Motors Based on Extended EMF Models Considering Magnetic Saturation With Online Parameter Identification," in *IEEE Transactions on Industry Applications*, vol. 42, no. 5, pp. 1264-1274, Sept.-Oct. 2006.

[7] Y. Zhao, Z. Zhang, W. Qiao and L. Wu, "An Extended Flux Model-Based Rotor Position Estimator for Sensorless Control of Salient-Pole Permanent-Magnet Synchronous Machines," in *IEEE Transactions on Power Electronics*, vol. 30, no. 8, pp. 4412-4422, Aug. 2015.

[8] F. Gao, Z. Yin, C. Bai, D. Yuan and J. Liu, "Speed Sensorless Control Method of Synchronous Reluctance Motor based on Resonant Kalman Filter," in *IEEE Transactions on Industrial Electronics*, 2022.

[9] F. Gao, Z. Yin, C. Bai, D. Yuan and J. Liu, "A Lag Compensation-Enhanced Adaptive Quasi-Fading Kalman Filter for Sensorless Control of Synchronous Reluctance Motor," in *IEEE Transactions on Power Electronics*, vol. 37, no. 12, pp. 15322-15337, Dec. 2022.

[10] Y. Zhang, Z. Yin, C. Bai, G. Wang and J. Liu, "A Rotor Position and Speed Estimation Method Using an Improved Linear Extended State Observer for IPMSM Sensorless Drives," in *IEEE Transactions on Power Electronics*, vol. 36, no. 12, pp. 14062-14073, Dec. 2021.

[11] Y. Zhao, W. Qiao and L. Wu, "Improved Rotor Position and Speed Estimators for Sensorless Control of Interior Permanent-Magnet Synchronous Machines," in *IEEE Journal of Emerging and Selected Topics in Power Electronics*, vol. 2, no. 3, pp. 627-639, Sept. 2014.

[12] X. Wu et al., "Enhanced Position Sensorless Control Using Bilinear Recursive Least Squares Adaptive Filter for Interior Permanent Magnet Synchronous Motor," in IEEE Transactions on Power Electronics, vol. 35, no. 1, pp. 681-698, Jan. 2020.

[13] Z. Yin, G. Li, Y. Zhang and J. Liu, "Symmetric-Strong-Tracking-Extended-Kalman-Filter-Based Sensorless Control of Induction Motor Drives for Modeling Error Reduction," in *IEEE Transactions on Industrial Informatics*, vol. 15, no. 2, pp. 650-662, Feb. 2019.

[14] S. Bolognani, R. Oboe and M. Zigliotto, "Sensorless full-digital PMSM drive with EKF estimation of speed and rotor position," in *IEEE Transactions on Industrial Electronics*, vol. 46, no. 1, pp. 184-191, Feb. 1999.

[15] D. Pasqualotto, S. Rigon and M. Zigliotto, "Sensorless Speed Control of Synchronous Reluctance Motor Drives Based on Extended Kalman Filter and Neural Magnetic Model," in *IEEE Transactions on Industrial Electronics*, vol. 70, no. 2, pp. 1321-1330, Feb. 2023.

[16] S. Bolognani, S. Calligaro and R. Petrella, "Design Issues and Estimation Errors Analysis of Back-EMF-Based Position and Speed Observer for SPM Synchronous Motors," in *IEEE Journal of Emerging and Selected Topics in Power Electronics*, vol. 2, no. 2, pp. 159-170, June 2014.